

Thermodynamic Assessment of the Mo–Si System

Andreas Klaus Czerny,* Wenhao Ma, Clemens Simon Hausner, Peter Franke, Magnus Rohde, and Hans Jürgen Seifert

The binary system Mo–Si is reassessed based on previously reported findings that the Mo₃Si phase shows a deficiency in Si and to take into account experimental data on the heat capacities of the Mo silicides. The last aspect in particular has been neglected in previous assessments of the system. Experimental studies are carried out which confirm that the Mo₃Si phase is deficient in Si in every alloy analyzed, with an average Si content of 23 at%. The thermodynamic description of this phase is adjusted accordingly and the parameters of the system are optimized. Two alternative possible descriptions are presented for the phase Mo₃Si. It is shown that the calculated binary phase diagram agrees well with experimental data, like liquidus and solidus temperatures as well as homogeneity ranges of the phases, where applicable, for both datasets. Likewise, thermophysical data like enthalpies of the formation of the silicides are adequately described.

1. Introduction

Mo–Si alloys have been investigated and developed extensively due to their diverse range of applications and intriguing properties. Alloys in this system exhibit excellent high-temperature strength, oxidation resistance, and potential for use in various industries, including aerospace applications, gas turbines, use as heating elements, and as structural materials in extreme environments.^[1–4] Considerable efforts have been taken to investigate the thermophysical and thermochemical properties of Mo–Si alloys, as a fundamental understanding of their phase equilibria and thermodynamic properties is essential for alloy design and optimization. Consequently, several thermodynamic assessments using the calculation of phase diagrams (CALPHAD) method have been conducted in attempts to model the Mo–Si system accurately, for example, the works by Guo et al.^[5] Vahlas et al.^[6] Liu et al.^[7] or Geng et al.^[8] For different

reasons, none of the existing CALPHAD assessments have provided entirely satisfying results. One of the challenges lies in the accurate representation of the intermetallic phase Mo₃Si. In the year 2000, Rosales and Schneibel^[9] have shown this phase to be deficient in silicon, with a Si content of about 23 at%. This result was later confirmed by other researchers, such as Gulec et al.^[10] and Gnesin and Gnesin.^[11] In addition, this off-stoichiometry was confirmed in several ternary systems containing Mo–Si, e.g., Mo–Si–Ti,^[12] Mo–Si–B,^[13] and Mo–Si–Cr.^[14] However, this fact has been disregarded in all previous assessments, leading to discrepancies between predicted and observed phase equilibria and thermodynamic properties. Another important aspect of the system which


was largely neglected in previous CALPHAD assessments is the heat capacities of the intermetallic phases. All published datasets use a simple Kopp–Neumann approach, which should only be used in lack of experimental heat capacity data. Thus, all current assessments of the system Mo–Si have shortcomings that impact their applicability in certain aspects.

The aim of this study is to provide a comprehensive reassessment of the Mo–Si system, resulting in an improved thermodynamic description. This investigation will experimentally reaffirm the silicon deficiency of Mo₃Si and incorporate this critical aspect into the thermodynamic assessment. A thorough evaluation of all available data from the literature, encompassing both experimental measurements and theoretical predictions, is presented. By combining new experiments with a wide range of reliable data, the aim is to establish a robust thermodynamic model that accurately reflects the Mo–Si system.

2. Literature Overview

The experimental phase diagram data that are available in the literature are listed in **Table 1**. Thermodynamic data of the system are listed in **Table 2** and **3** for experimental and calculated data, respectively. In the following sections, aspects of these data, as well as previous assessments of the system Mo–Si, will be discussed. It should be noted that the objective is not a definitive and complete review of previous literature. Rather, relevant aspects of certain publications and experiments pertaining to this assessment are discussed. For detailed reviews, the reader is referred to the publications by Gokhale and Abbaschian^[15] or Schlesinger.^[16]

A. K. Czerny, W. Ma, C. S. Hausner, P. Franke, M. Rohde, H. J. Seifert
Institute for Applied Materials - Applied Materials Physics (IAM-AWP)
Karlsruhe Institute of Technology
Hermann-von-Helmholtz-Platz 1, 76344 Eggenstein- Leopoldshafen,
Germany
E-mail: andreas.czerny@kit.edu

 The ORCID identification number(s) for the author(s) of this article can be found under <https://doi.org/10.1002/adem.202302085>.

© 2024 The Authors. Advanced Engineering Materials published by Wiley-VCH GmbH. This is an open access article under the terms of the Creative Commons Attribution-NonCommercial License, which permits use, distribution and reproduction in any medium, provided the original work is properly cited and is not used for commercial purposes.

DOI: 10.1002/adem.202302085

Table 1. Experimental phase diagram data of the Mo–Si system.

Literature	Method	Equilibria	Temperature [K]	Si [at%]
Gnesin and Gnesin ^[11]	Metallography, EDX, X-ray	Composition of Mo ₃ Si	1753–1973	25
Gulec et al. ^[10]	Z-contrast imaging, electron diffraction, atom probe tomography	Composition and structure of Mo ₃ Si	(cast sample not annealed)	25
Rosales and Schneibel ^[9]	Metallography, EDX, X-ray	Composition of Mo ₃ Si	1600	22–28
Frankwicz and Perepezko ^[20]	Metallography, EDX, X-ray	Phase equilibria and stability of MoSi ₂	RT - 2173	55, 60, 67
Svechnikov et al. ^[19]	DTA, X-ray, metallography	Liquidus, eutectics, peritectic, solidus, Si-solubility in Mo and Mo ₅ Si ₃	1673–ca. 2600	0–100
Kieffer and Cerwenka ^[18]	Pyrometry, metallography, X-ray	Liquidus	1673–2873	0–100
Ham ^[17]	X-ray	Si-solubility in Mo	1588–1700	0.8–2.7
Cherniak and Elliot ^[21]	X-ray, pyrometry, metallography	MoSi ₂ , Mo ₅ Si ₃	1973–2273	66.6

Table 2. Experimental thermodynamic investigations of the Mo–Si system.

Literature	Method	Type of data	Temperature [K]	Si [at%]
Fujiwara and Ueda ^[31]	EMF	Enthalpies and entropies of formation of Mo ₃ Si, Mo ₅ Si ₃ , MoSi ₂	1305–1507	25, 37.5, 66.6
Meschel and Kleppa ^[62]	Direct synthesis calorimetry	Enthalpies of formation of Mo ₅ Si ₃ , MoSi ₂	1473	37.5, 66.6
Tomaskiewicz et al. ^[29]	Combustion calorimetry	Enthalpy of formation of Mo ₅ Si ₃	298	37.5
Callanan et al. ^[45]	Adiabatic calorimetry	Heat capacity	7–392	66.6
Tomaskiewicz et al. ^[30]	Combustion calorimetry	Enthalpy of formation of Mo ₃ Si	298	25
O'Hare ^[28]	Combustion calorimetry	Enthalpy of formation of MoSi ₂	298	66.6
Arpaci and Froberg ^[42]	Pyrometry	Integral enthalpy of mixing (liquid phase)	3087	0–40
Ohmori et al. ^[63]	EMF	Standard Gibbs energies of formation of Mo ₃ Si, Mo ₅ Si ₃	1150–1450	25, 37.5
Maslov et al. ^[64]	Direct synthesis calorimetry	Enthalpy of formation of MoSi ₂	No temperature is given in this article.	66.6
Chart ^[27]	Knudsen effusion	Gibbs energies, enthalpies and entropies of formation and heat capacities of Mo ₃ Si, Mo ₅ Si ₃ , MoSi ₂	1410–1675	20, 35, 60
Bondarenko et al. ^[48]	Calorimetry (displacement method)	Enthalpy	1200–2200	25, 37.5, 66.6
Bondarenko et al. ^[49]	Adiabatic calorimetry	Heat capacity	400–1200	25, 37.5, 66.6
Searcy and Tharp ^[26]	Knudsen effusion	Enthalpies of formation of Mo ₃ Si, Mo ₅ Si ₃ , MoSi ₂	1926–2261	25, 37.5, 66.6
King and Christensen ^[41]	Calorimetry	Heat capacity, enthalpy	51–289 (Heat capacity), 400–1451 (Enthalpy)	25
Walker et al. ^[46]	Drop calorimetry	Heat capacity	303–1173	66.6
Robins and Jenkins ^[25]	Combustion calorimetry	Enthalpy of formation of MoSi ₂	298	66.6
Douglas and Logan ^[44]	Ice calorimetry	Heat capacity	273–1173	66.6

Table 3. Calculated thermodynamic data of the Mo–Si system.

Literature	Method	Type of data
Pan ^[38]	First-principles calculations	Debye temperature, heat capacity (C _v) of Mo ₅ Si ₃
Zhong et al. ^[36]	First-principles calculations	Debye temperature, heat capacity (C _v), thermal expansion of Mo ₃ Si
Colinet and Tedenac ^[37]	First-principles calculations	Enthalpies of formation of Mo ₃ Si, Mo ₅ Si ₃ , MoSi ₂
Bhaduri et al. ^[34]	Calculation	Enthalpies of formation of Mo ₅ Si ₃ , MoSi ₂
Birnie et al. ^[65]	Pair potential calculations	Enthalpies of formation of the Mo–Si solid solution
Niessen and de Boer ^[33]	Miedema	Enthalpies of formation of Mo ₃ Si, MoSi ₂
Machlin ^[66]	Modified Miedema	Enthalpy of formation of Mo ₃ Si
Kaufman ^[67]	Prediction	Enthalpies of formation of Mo ₃ Si, Mo ₅ Si ₃ , MoSi ₂

2.1. Phase Diagram Data

Relevant phase diagram data for the system Mo–Si can be traced back to 1951, when Ham reported the solubility of Si in Mo.^[17] In 1952, Kieffer and Cerwenka^[18] measured liquidus temperatures of 22 samples within the system, covering the whole composition range. In that work, the intermetallic phases are identified as Mo₃Si, Mo₃Si₂, and MoSi₂. It was later found in a study by Svechnikov et al.^[19] that the phase denoted as Mo₃Si₂ by Kieffer and Cerwenka^[18] is instead Mo₅Si₃. The same publication by Svechnikov et al. provides a comprehensive study of the phase equilibria of the system and presents data for all invariant reactions, liquidus and solidus temperatures, and Si solubilities in Mo and Mo₅Si₃. The phase Mo₅Si₃ was reported to have a homogeneity range, extending from about 36.5 at% to 39 at%. The authors also included a presumed polymorphic transformation of the MoSi₂ phase at 2173 K, from a tetragonal C11_b structure to a hexagonal C40 structure (notation according to the Strukturbericht). In 1998, Frankwicz and Perepezko^[20] studied the phase stability of MoSi₂ at high temperatures. The experiments proved that the C40 structure is metastable and thus must not be included in the phase diagram. Aside from this phase transformation, the data from Svechnikov et al. and Kieffer and Cerwenka only show significant differences in two more regards. For once, the eutectic reaction $L \rightleftharpoons \text{Mo}_3\text{Si} + \text{Mo}_5\text{Si}_3$ occurs at 2293 K and 26.4 at% according to Svechnikov et al. while Kieffer and Cerwenka reported a temperature of 2200 K and a Si concentration of 32.4 at% in the liquid phase. Second, the solubility of Si in Mo is nearly twice as high according to Svechnikov et al. as was measured by Kieffer and Cerwenka. As Gokhale and Abbaschian pointed out in an assessment of the system,^[15] the data of Svechnikov should be preferred in this case, owing to more extensive experimentation and better experimental equipment. Lastly, in 1964, Cherniack and Elliot^[21] studied the high-temperature behavior of the phases Mo₅Si₃ and MoSi₂. In this publication, they reported the melting points of Mo₅Si₃ and MoSi₂ to be 2358.15 and 2253.15 K, respectively, and the eutectic temperature involving Mo₅Si₃ and MoSi₂ to be 2173.15 K. However, they reported experimental issues in this study, such as considerable evaporation of Si in the MoSi₂-containing samples, which affected the measurements.

In 2000, Rosales and Schneibel^[9] reported that the phase Mo₃Si is not stoichiometric, as was presumed until then, but has a slightly lower Si concentration “near 24 at%” for a sample that was annealed at 1873 K. In 2016, Gulec et al.^[10] confirmed the off-stoichiometry of this phase. The samples observed in this study, however, seem to have been analyzed in the cast state, with no annealing prior to analysis. Lastly, in 2020, Gnesin and Gnesin^[11] studied the composition of several Mo–Mo₃Si samples produced by various methods (sintering in one or more steps, levitation melting with and without annealing) and consistently found that the Si concentration of the A15 phase is about 23 at%.

2.2. Thermodynamic Data

Several reviews of the thermodynamic data of the Mo–Si system exist in literature, for example, the ones by

Chandrasekharaiah et al.^[22] Schlesinger,^[16] Brewer and Lamoreaux,^[23] or Chart.^[24] These reviews give a detailed overview of the available literature, but certain publications, or aspects thereof, will be discussed in the following section. One thermodynamic parameter will be discussed per subsection, pointing out relevant discrepancies, peculiarities, etc. For a detailed and complete literature review, the aforementioned articles are recommended. No CALPHAD assessments are taken into account in this section.

2.2.1. Enthalpy of Formation

Aside from early publications, the enthalpies of formation of the intermetallic phases, obtained experimentally, show remarkably little variation between different studies. In 1955, Robins and Jenkins^[25] published results of Mo₅Si₃ (which was at the time assumed to be Mo₃Si₂) and MoSi₂, obtained from combustion calorimetry. However, due to rather impure raw materials, these measurements are not considered reliable nowadays. In 1960, Searcy and Tharp^[26] measured the dissociation pressures and enthalpies of the formation of all three intermetallic compounds of the system via Knudsen effusion. However, these measurements are also considered unreliable due to interaction of the specimen with the container, sintering of the sample, and, as Chandrasekharaiah et al.^[22] comment, a high probability that the specimens were not in equilibrium at the chosen conditions. In 1974, Chart^[27] published a study regarding the enthalpies of formation of all three intermetallic compounds measured with Knudsen effusion as well. The difficulties of the previous studies were accounted for and Chart reported values which are still considered highly trustworthy. In fact, the measurements are used in CALPHAD assessments of the Mo–Si system to this day. It must be noted, however, that Chandrasekharaiah et al.^[22] recommended that larger uncertainties should be assigned to the values obtained by Chart. The vast majority of measurements since then, for example, the three related articles by O’Hare^[28] for MoSi₂ and Tomaskiewicz et al. for Mo₃Si^[29] and Mo₅Si₃,^[30] respectively, or by Fujiwara and Ueda,^[31] have confirmed the values by Chart. O’Hare and Tomaskiewicz et al. used combustion calorimetry, while Fujiwara and Ueda used electromotive force (EMF) measurements. In both cases, the obtained values are within the uncertainty of measurement of the experiments by Chart.

For modeling and theoretical calculation of the enthalpies of the formation of Mo silicides, the results vary strongly depending on the method used. Predictions with the Miedema model^[32] for this system are rather unreliable, as shown by Niessen and de Boer^[33] in 1981. Bhaduri et al.^[34] calculated the enthalpies of formation of Mo₅Si₃ and MoSi₂ by using values of the heat capacities (taken as listed by Barin^[35]) and obtained results that are close to experimental values. For ab initio methods, three articles are available to our best knowledge. In 2016, Zhong et al.^[36] published results concerning structural, elastic, and thermodynamic properties calculated by density functional theory (DFT) for Mo₃Si and Mo₃Ge. However, both for the generalized gradient approximation and for local density approximation, the reported enthalpies of formation differed significantly from the experimental results. In the same year, Colinet and Tedenac^[37] published enthalpies of formation of several transition metal

compounds calculated with DFT. Those results were close to experimental results in case of the Mo-silicides. In 2019, Pan^[38] used DFT to calculate the enthalpy of formation of Mo_5Si_3 and reported a result that is within the experimental uncertainty reported by Chart.^[27]

2.2.2. Entropy of Formation

Apart from the CALPHAD evaluations of the system, data on the entropies of formation of the intermetallic phases in the Mo–Si system are scarce. To the best of our knowledge, there are only two experimental sources: the publications by Chart in 1974^[27] and by Fujiwara and Ueda in 2007.^[31] As mentioned above, Chart analyzed the intermetallic phases by Knudsen effusion experiments, while Fujiwara and Ueda used EMF measurements. Although the entropies of formation are not explicitly reported in Fujiwara and Ueda's article, they can be calculated from the data presented. Unlike the reported enthalpies of formation, there are significant discrepancies in the reported values of the entropies of formation of all three intermetallic compounds between the two publications.

Another way to obtain values for the entropies of formation of the intermetallic compounds is to calculate them from reported entropies of the phases and the unary data compiled by Dinsdale.^[39] For the system Mo–Si, this is possible using the data from Callanan et al.^[40] for MoSi_2 and King and Christensen^[41] for Mo_3Si , respectively. From these experiments, the derived entropies of formation at 298 K (referring to 1 mole of atoms) are $0.446 \text{ J mol}^{-1} \text{ K}^{-1}$ for Mo_3Si and $-1.57 \text{ J mol}^{-1} \text{ K}^{-1}$ for MoSi_2 . However, these values deviate fairly strongly from both the data reported by Chart and the data derived from Fujiwara and Ueda.

In conclusion, interpretation of the entropies of formation for the intermetallic compounds in the Mo–Si system should be done with caution, given the limited data and the marked differences in results between publications.

2.2.3. Enthalpy of Mixing

Arpaci and Froberg^[42] studied the mixing enthalpy of the liquid in the system Mo–Si in 1985. The experiment was carried out using a levitation apparatus in which molten Mo was held in a suspended state and Si was introduced by controlled drops from a revolver magazine. The experimental temperature was maintained at a mean value of 3087 K (scattering from 2960 to 3224 K), with concentrations ranging from 0 to 40 at% Si. The enthalpy of mixing was derived from the resulting temperature change. The calculation required an estimation of the heat capacity, which was obtained using the Kopp–Neumann approach. For temperature measurements, a pyrometer was used. Notably, the spectral emissivity of pure Mo was utilized due to the unavailability of values for molten Mo–Si alloys. Hence, the authors acknowledged the inherent accumulating error associated with the progressive addition of Si and made the decision to retain it as acceptable. The total systematic error of the experiment is stated to be within $\pm 12\%$ for the enthalpy of mixing.

Also in 1985, Sudavtsova et al.^[43] published measurements regarding the enthalpies of mixing in several binary Si-metal melts, among them Mo–Si with up to 8 at% Mo. The values were experimentally determined using a calorimeter and the temperature chosen for the Mo–Si specimens was 1870 K. Little other information regarding purity of the components, experimental techniques, or possible errors are given in the article. For this reason, the data were disregarded for the optimization.

2.2.4. Heat Capacity

Reliable information on the heat capacities of Mo–Si compounds is surprisingly scarce in the literature. Douglas and Logan,^[44] Callanan et al.^[45] and Walker et al.^[46] measured the heat capacity of MoSi_2 . Mezaki et al.^[47] published enthalpy increment values of the same compound. King and Christensen^[41] published heat capacity as well as enthalpy increment data of Mo_3Si . Finally, Bondarenko et al.^[48,49] reported enthalpy increment values and heat capacity data for all three intermetallic compounds. In 1972, they reported data ranging from 400 to 1200 K, in 1973, data were published spanning the range from 1200 to 2200 K. Significant differences exist in the data between the two publications, as well as between the the data from 1972 and measurements by other authors. The data from 1973, however, agrees fairly well with data published by the other authors. For this reason, the data from 1972 were disregarded for this optimization.

2.3. Previous Assessments

The following section discusses previous assessments of the Mo–Si system. This includes publications using the CALPHAD method as well as those using traditional phase diagram evaluation methods.

Vahlas et al.^[6] published thermodynamic evaluations of several Si-metal binary systems in 1989. They used the CALPHAD method and compared the results of the calculations with experimental findings. This publication is noteworthy due to the fact that it is the first one that resulted in a set of optimized parameters for calculating the Gibbs energies of all phases. However, many of the invariant reactions they calculated are not observed experimentally, particularly in the Mo-rich area of the system. In addition, for high Si contents, the liquid phase showed a miscibility gap at high temperatures.

A widely regarded thermodynamic assessment of the Mo–Si system was published by Gokhale and Abbaschian.^[15] The authors discussed the literature up to the year 1991 extensively. As mentioned in Section 2.1, the phase diagram data of Svechnikov et al.^[19] are trusted over the data of Kieffer and Cerwenka^[18] due to better experimental techniques of the former. The resulting phase diagram was the first widely accepted publication which included the homogeneity range of the phase Mo_5Si_3 . However, the authors also included the presumed polymorphic transformation of MoSi_2 .

In 1994, Costa e Silva^[50] published an assessment of the Mo–Si system as part of a doctoral thesis. The topic of the thesis was the synthesis of MoSi_2 composites. The author stated the work was necessary due to the aforementioned miscibility gap

in Vahlas' work. The data assessed by Chart,^[24] Brewer and Lamoreaux,^[23] and Gokhale and Abbaschian were accepted. All intermetallic phases were treated as line compounds. Similar to the work by Vahlas, many of the invariant reactions calculated by Costa e Silva are not supported by experimental investigations any longer.

In 2000, as part of the evaluation of the ternary Al–Mo–Si system, the Mo–Si system was evaluated by Liu et al.^[7] This description agrees well with most of the data that were available at the time, but it has several shortcomings. For instance, the temperatures of the invariant reactions are in some cases significantly lower than the experimental values. In addition, at high temperatures, the homogeneity range of the phase Mo₅Si₃ shows rather unrealistic behavior.

In 2010, Geng et al.^[8] reassessed the Mo–Si system to obtain a description of the ternary system Nb–Si–Mo. The off-stoichiometry of Mo₃Si, reported by Rosales and Schneibel^[9] in 2000, was disregarded and not mentioned in the article. One stated aim of the assessment was to make the description of the iso-structural phases Nb₅Si₃ and Mo₅Si₃ compatible, as they form a continuous solid solution. Therefore, the authors changed the description of the phase Mo₅Si₃ by modeling it using three sublattices, accepting the description of Nb₅Si₃ by Fernandes et al.^[51] However, as Fernandes et al. themselves state, the phase would correctly be described in four sublattices, one corresponding to each Wyckoff position. The simplification is only viable if there are no defects in the Si positions, which is true for Nb₅Si₃, but not for Mo₅Si₃.

The latest assessment of the Mo–Si system to date was published by Guo et al.^[5] in 2012. The aim was a reassessment of the Al–Mo–Si system, implementing the same improved description of the phase Mo₅Si₃ that was published by Geng et al. two years prior. While this did improve the calculations for the ternary system, the enthalpy of formation of the phase MoSi₂ calculated by this dataset deviates significantly from the experimental values. Furthermore, like the previous publications, this assessment did not take into account the silicon deficiency of the phase Mo₃Si.

3. Thermodynamic Models and Phase Descriptions

For the pure elements Mo and Si, the Gibbs energy functions are taken from the SGTE unary database compiled by Dinsdale.^[39] The Mo–Si system contains six phases: the liquid phase, the Mo-based solid solution (bcc-phase), silicon and the three intermetallic phases Mo₃Si, Mo₅Si₃, and MoSi₂. The phases liquid and bcc are described as solution phases. The intermetallic phase MoSi₂ is described as stoichiometric phase. The compound Mo₅Si₃, is described by a sublattice model expressed in the compound energy formalism.^[52,53] For the phase Mo₃Si, two alternative descriptions are used. In one dataset, this phase is described as a simple stoichiometric phase with the experimentally observed composition of 23 at% Si. Alternatively, the phase is described in three sublattices; one containing Mo, one containing Si, and one containing Si and vacancies. In the following section, the reasoning behind each chosen model is described. A brief overview of the sublattice model is also given. An in-depth explanation of the compound energy formalism can be found in

Table 4. Crystallographic information about the solid phases in the Mo–Si system. For Mo₃Si, see Section 3.2.3.

Phase	Pearson symbol	Space group	Strukturbericht	Prototype
bcc	cI2	Im $\bar{3}$ m, #229	A2	W
Si	cF8	Fd $\bar{3}$ m, #227	A4	Diamond
Mo ₃ Si	cP8	(Pm $\bar{3}$ n, #223)	(A15)	Cr ₃ Si
Mo ₅ Si ₃	tI32	I4/mcm, #140	D8 _m	W ₅ Si ₃
MoSi ₂	tI6	I4/mmm, #139	C11 _b	MoSi ₂

ref. [54]. Relevant crystallographic information of all phases used in this work is summarized in **Table 4**.

3.1. Solution Phases

The molar Gibbs energies of the phases with homogeneity range are described by the following equation:

$$G_m^\phi(T) = x_{\text{Mo}} G_{\text{Mo}}^\phi(T) + x_{\text{Si}} G_{\text{Si}}^\phi(T) + RT(x_{\text{Mo}} \ln x_{\text{Mo}} + x_{\text{Si}} \ln x_{\text{Si}}) + {}^{\text{ex}} G_m^\phi \quad (1)$$

where x_{Mo} and x_{Si} are the mole fractions of the elements molybdenum and silicon, respectively. ${}^{\text{ex}} G_m^\phi$ is the excess Gibbs energy, which is expressed by a Redlich–Kister polynomial:

$${}^{\text{ex}} G_m^\phi = x_{\text{Mo}} x_{\text{Si}} \sum_j L_{\text{Mo,Si}}^\phi (x_{\text{Mo}} - x_{\text{Si}})^j \quad (2)$$

3.2. Intermetallic Compounds Described in the Sublattice Model

In the sublattice model, the Gibbs energy is calculated with the following equation:

$$G_m = G_m^{\text{ref}} + G_m^{\text{id}} + G_m^{\text{ex}} \quad (3)$$

where G_m^{ref} is the Gibbs energy reference, G_m^{id} is the term corresponding to ideal mixing and G_m^{ex} is the excess Gibbs energy, respectively.

The reference state assumes an unreacted mixture of the constituents of the phase. Its contribution is given by:

$$G_m^{\text{ref}} = \sum_I P_I(Y) {}^0 G_I \quad (4)$$

where I stands for a component array specifying one constituent in each sublattice, $P_I(Y)$ is the product of the constituent fractions, and ${}^0 G_I$ is the Gibbs energy of the compound I .

The second term in Equation (3) corresponds to the ideal mixing entropy, which assumes one component on each sublattice and no interaction between atoms. It is calculated by the equation:

$$G_m^{\text{id}} = RT \sum_S a^S \sum_i \gamma_i^S \ln \gamma_i^S \quad (5)$$

where a^S is the number of sublattice sites and y_i^S is the constituent fraction of the component on that sublattice.

Finally, the excess term takes into account all interactions between the constituents which affect the Gibbs energy of the phase. Mathematically, it is the sum of the interaction parameters L_{IZ} defined by component arrays of the Z th order:

$$G_m^{\text{ex}} = \sum_{Z>0} \sum_{IZ} P_{IZ}(Y) L_{IZ} \quad (6)$$

3.2.1. MoSi₂

The space group of the phase MoSi₂ is $I4/mmm$. Si atoms occupy the Wyckoff position 4e on the lattice while Mo atoms occupy the position 2a. No significant substitution is reported. Thus, the phase is described as a line compound: (Mo)₁ (Si)₂. Consequently, no interaction parameters are used to describe the molar Gibbs energy of this phase.

3.2.2. Mo₅Si₃

The space group of the phase Mo₅Si₃ is $I4/mcm$. At stoichiometric composition ($x(\text{Si}) = 37.5$ at%), the Mo atoms occupy the Wyckoff positions 16k and 4b, while the Si atoms occupy the 4a and 8h positions.^[55] At Si deficiency, the Si atoms at the 4a positions are partially substituted by Mo, whereas at Si excess, the Mo atoms at the 4b positions are partially substituted by Si.^[56] To adequately describe this behavior, this phase was modeled with four sublattices. Each Wyckoff position corresponds to one sublattice: (Mo)_{0.5}(Mo, Si)_{0.125}(Mo, Si)_{0.125}(Si)_{0.25}, where the majority atom is underlined, if applicable.

3.2.3. Mo₃Si

The crystal structure of Mo₃Si was determined by Templeton and Dauben^[57] from X-ray powder diffractograms. It is isostructural with Cr₃Si and has the Strukturbericht designation A15 (space group $Pm\bar{3}n$, #223). Accordingly, Si occupies the corners and the center of the cubic unit cell (Wyckoff position 2a), while two Mo atoms can be found on each of the faces of the unit cell (Wyckoff position 6c).

However, forbidden reflections were detected in electron diffraction images of various compounds with an A15 structure (Nb₃Al, Cr₃Si, V₃Si), which indicates a superstructure in these crystals.^[58] It is known from the phase diagrams of these systems that the compounds related to the A15 structure have solubility ranges that are particularly extended toward the excess component side. Therefore^[58] came to the conclusion that by incorporating defects (vacancies or antistructure atoms) on only one of the two Si positions (or Al positions in Nb₃Al, respectively), the symmetry of the crystals is reduced (space group $Pm\bar{3}$, #200) and the reflections in question are now permitted. However, a decision about the dominant defect type (vacancies or antistructure atoms) could not be reached.

Additional information about the nature of the prevailing defects can be derived from diffusion experiments, as reported by Prasad and Paul.^[59] In this work, the growth of Mo silicides in

diffusion pairs was examined, and from the evaluation of the diffusion coefficients it was concluded that in Mo₃Si there must be a very high concentration of vacancies in the Si sublattice, but also a significant content of Mo antistructure atoms. Since the focus in the present work is on the thermodynamic description of the phases and there are very few experimental results on the compositional range of the Mo₃Si phase, the present phase model for Mo₃Si takes into account only the dominant type of defects, i.e. vacancies. The structural model is derived from the A15 unit cell, although the two Si positions are no longer equivalent because the Si in the center of the unit cell is partially replaced by vacancies. The structure should therefore belong to the space group $Pm\bar{3}$ and consist of 3 sublattices belonging to the following Wyckoff positions: (1a) Si on the corners of the unit cell, (1b) Si and vacancies in the center, and (6f) two Mo atoms on each face of the unit cell. Regarding this structural model, however, it should be noted that recent electron diffraction studies on Mo₃Si using a transmission electron microscopy (TEM)^[10] have shown that the structure of Mo₃Si does not have cubic translational symmetry due to incommensurable modulations. However, we assume that the incommensurable superstructure only shifts the lattice positions, but does not change their occupation numbers, so that our sublattice and defect model proposed here is still applicable. To summarize the results reported in the literature, while there is strong evidence from diffusion experiments that the Si deficiency of the Mo₃Si phase is due to vacancies, antisite atoms cannot be conclusively excluded. For this reason, two alternative models for the phase Mo₃Si are presented in this work. In one dataset, this phase is described as a simple stoichiometric compound with the experimentally observed composition: (Mo)_{0.77}(Si)_{0.23}. In the second dataset, the phase is described in three sublattices, taking into account vacancies: (Mo)₆(Si)(Si,Va).

4. Results and Discussion

4.1. Experimental Results

The nominal compositions of the alloys are analyzed in this work, as well as the phases which are expected to be present according to the phase diagram are listed in **Table 5**. SEM pictures, taken in backscattered electron (BSE) mode, of the samples after annealing at 1300 °C for 330 h are shown in **Figure 1**. For EPMA, care was taken to position the beam in a way that minimized the possibility of inadvertently measuring the surrounding phase. Generally, in the studied alloys, all phases are sufficiently large in size for a sound analysis.

Table 5. The nominal compositions and the expected phases of the alloys investigated in this work.

Alloy number	Mo [at%]	Si [at%]	Expected phases
1	85	15	bcc + Mo ₃ Si
2	80	20	bcc + Mo ₃ Si
3	70	30	Mo ₃ Si+Mo ₅ Si ₃
4	65	35	Mo ₃ Si+Mo ₅ Si ₃

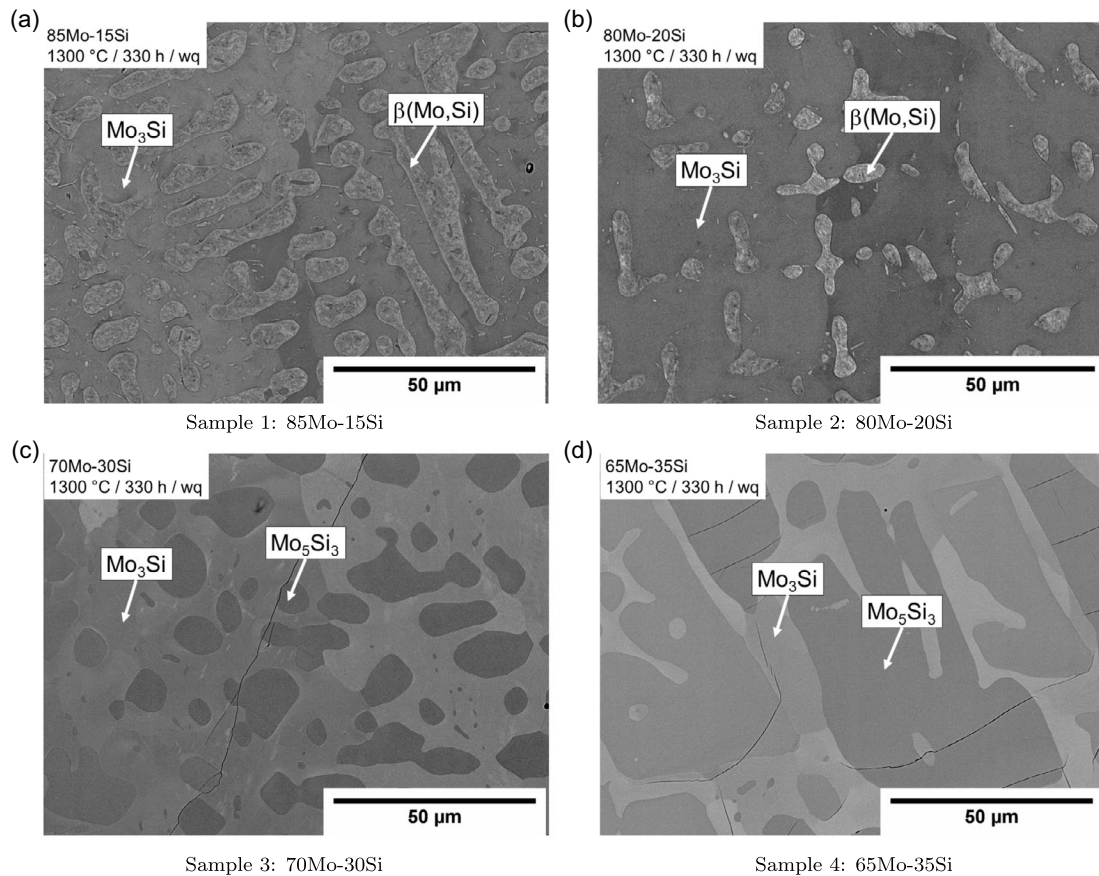


Figure 1. BSE images of the microstructures of the samples after annealing at 1300 °C for 330 h and quenching. a) 85Mo-15Si, b) 80Mo-20Si, c) 70Mo-30Si, and d) 65Mo-35Si.

The measured compositions of the phases of each alloy are listed in **Table 6**. All phase compositions are well within the expected range. The phase Mo_5Si_3 shows a slightly lower Si-content than the stoichiometric 37.5 at%. However, the standard deviations are 0.7 at% for sample 3 and 0.2 at% for sample 4, respectively, placing the results well within the reported homogeneity range of the phase. The composition of the Mo-based solid solution is consistent with the results reported in literature as well: 1.8 at% for sample 1 and 1.5 at% for sample 2 (standard deviations: 0.2 at% and 0.1 at%, respectively). For the phase

Table 6. The phase compositions for each sample, as determined by EPMA.

Alloy number	Detected phases	Mo [at%]	Si [at%]
1	bcc	98.2 ± 0.1	1.8 ± 0.1
	Mo_3Si	75.9 ± 0.5	24.1 ± 0.5
2	bcc	98.5 ± 0.2	1.5 ± 0.2
	Mo_3Si	77.3 ± 0.5	22.7 ± 0.5
3	Mo_3Si	76.9 ± 0.7	23.1 ± 0.7
	Mo_5Si_3	62.9 ± 0.7	37.1 ± 0.7
4	Mo_3Si	77.2 ± 0.2	22.8 ± 0.2
	Mo_5Si_3	63.0 ± 0.2	37.0 ± 0.2

Mo_3Si , the experiments confirm earlier findings from the literature.^[9–11] The phase shows a deficiency in Si, with a mean Si-content of ca. 23 at%. This is confirmed both for alloys in the two-phase region $\text{bcc} + \text{Mo}_3\text{Si}$ and the adjacent two-phase region $\text{Mo}_3\text{Si} + \text{Mo}_5\text{Si}_3$. The standard deviation of the measurements was 0.5 at%. Thus, the phase does not appear to have a significant homogeneity range.

The X-ray diffraction patterns are shown in **Figure 2**. For both samples in the two-phase region $\text{bcc} + \text{Mo}_3\text{Si}$ (Figure 2a,b), only the expected phases are present. For the samples in the two-phase region $\text{Mo}_3\text{Si} + \text{Mo}_5\text{Si}_3$ (Figure 2c,d), in addition to the two expected phases, there are also trace amounts of the Mo-based solid solution visible in the diffractograms. It is unclear if this is due to an insufficient heat treatment, or remnants from the outer layer of the sample which was affected by oxygen in the furnace. Regardless, the intensity of these peaks is very low, and no traces of the Mo-based solid solution could be detected by SEM or EPMA. Thus, it can be concluded that the effect of this phase is negligible.

4.2. Assessment Procedure

For the thermodynamic assessment, the PARROT module of the software Thermo-Calc^[60] is used. It allows the user to take into account a variety of different experimental results and apply

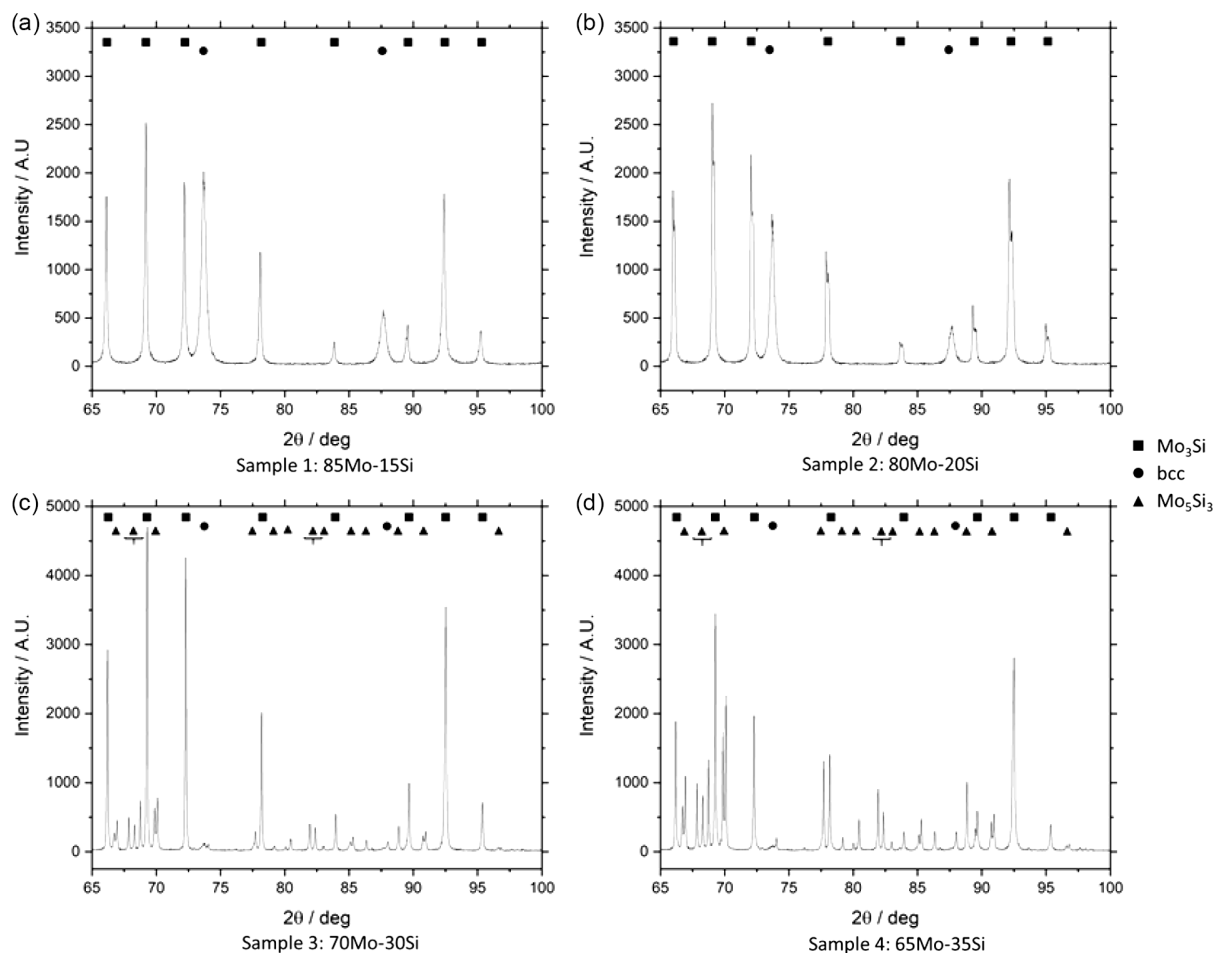


Figure 2. X-ray diffraction patterns of the samples after annealing at 1300 °C for 330 h and quenching. a) 85Mo-15Si, b) 80Mo-20Si, c) 70Mo-30Si, d) 65Mo-35Si.

weighing factors during the optimization of the variables, depending on the reliability of the data in question. During the optimization process, an error sum, which is calculated from the squared differences between the experimental data points and the calculated results, is minimized. This means that the parameters of the dataset are varied, until the error square sum is minimized. First, the parameters of each phase were optimized separately. Then all parameters were optimized simultaneously for the entire data set. The heat capacity data were optimized first, followed by the invariant reactions. Then the parameters of the Mo_5Si_3 phase were optimized. In particular, the parameter $G_{\text{Mo}_5\text{Si}_3:\text{Si}_3}$ was adjusted to the Si-rich border of the homogeneity range, while the parameter $G_{\text{Mo}_5\text{Si}_3:\text{Mo}_5\text{Si}_3}$ is most sensitive to the Mo-rich border. Then the homogeneity range of the Mo_5Si_3 phase was optimized, then the solidus, solvus, and liquidus data. Finally, all thermochemical and compositional data were optimized together.

The following sections lists the experimental data that were used for the optimization. For the heat capacity and enthalpy data, the publications of King and Christensen,^[41] Douglas and Logan,^[44] Walker et al.^[46] Callanan et al.^[45] Mezaki et al.^[47] and Bondarenko et al.^[48] were used. The liquidus and solidus temperatures of the system were taken from

Svechnikov et al.^[19] The same publication was used for the invariant reactions (both in terms of reaction temperature and phase composition) and to determine the homogeneity range of Mo_5Si_3 . For the solvus line of the Mo-based solid solution, the experimental data of Ham^[17] were also considered. For the data regarding the enthalpies of formation of the intermetallic phases, the data by Chart^[27] were accepted. Although several authors have published results which are considered reliable, because of the high agreement of the data across authors, only one set of formation enthalpy data has been used. Data for the enthalpy of mixing of the liquid phase were accepted from Arpaci and Frohberg.^[42] The temperatures and compositions of the invariant reactions, as well as the enthalpies of formation of the silicides, were generally given a higher weight than the other data points.

4.3. Thermodynamic Calculations

Figure 3 and **4** show the phase diagrams of the Mo-Si system optimized in the present work, along with the experimental data which are used for the optimization. In **Figure 3**, the phase Mo_3Si is modeled as a stoichiometric compound, while in

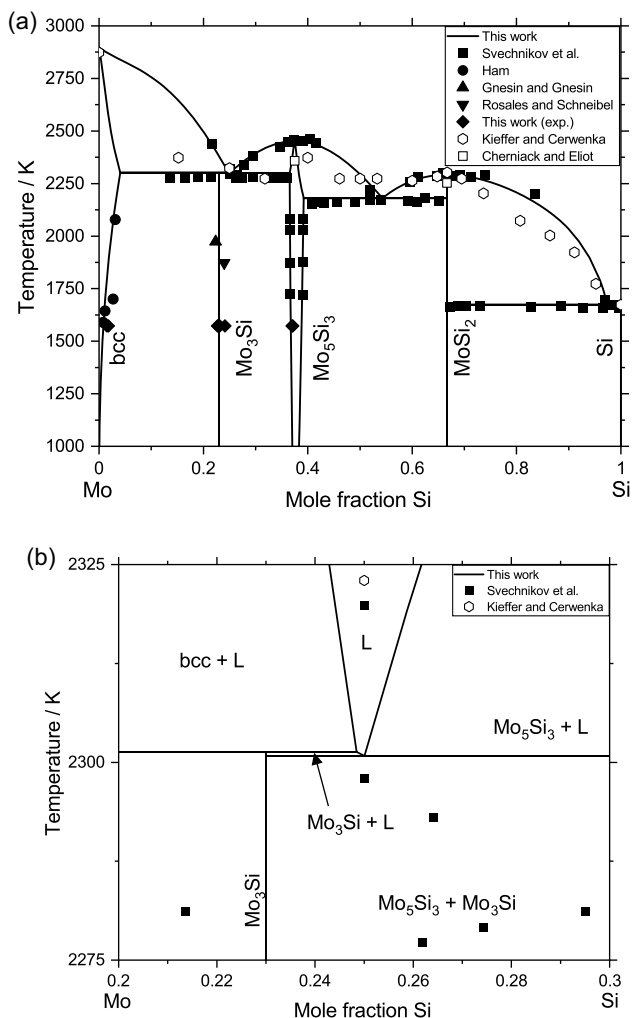


Figure 3. The phase diagram was calculated as a result of this work, with the phase Mo_3Si modeled as a stoichiometric compound. The data are the reported experimental values by Ham,^[17] Svechnikov et al.^[19] Gnesin and Gnesin,^[11] Rosales and Schneibel,^[9] Kieffer and Cerwenka,^[18] Cherniak and Elliot,^[21] and the experimental data from this work. Black points were used in the optimization, white points were disregarded. a) shows the entire phase diagram, b) is a detailed view of the section between 20 and 30 at.% Si.

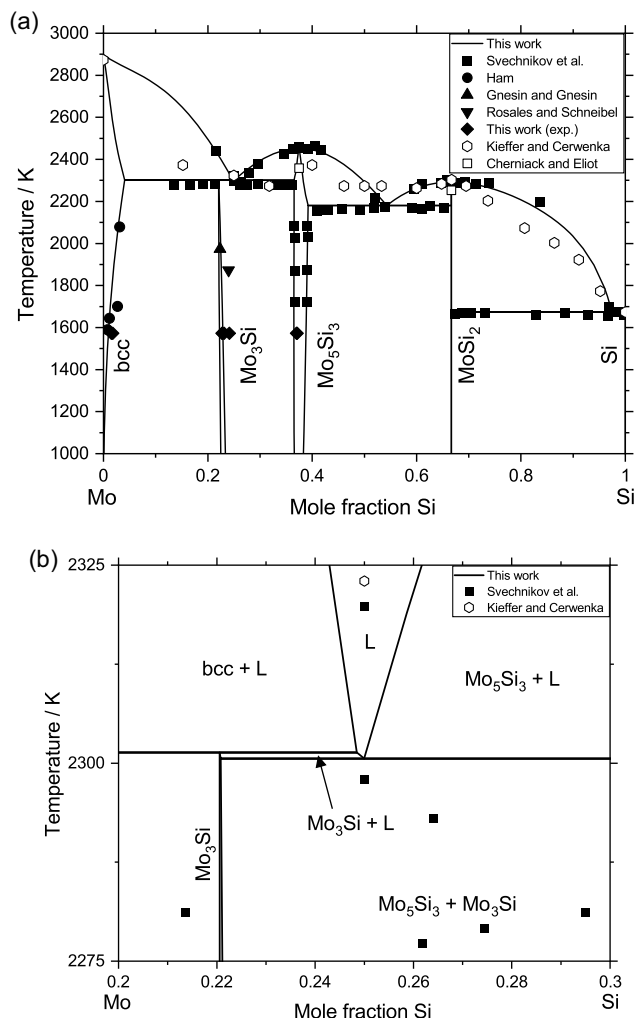


Figure 4. The phase diagram calculated as a result of this work, with the phase Mo_3Si described by a sublattice model. The data are the reported experimental values by Ham,^[17] Svechnikov et al.^[19] Gnesin and Gnesin,^[11] Rosales and Schneibel,^[9] Kieffer and Cerwenka,^[18] Cherniak and Elliot,^[21] and the experimental data from this work. Black points were used in the optimization, white points were disregarded. a) shows the entire phase diagram, b) is a detailed view of the section between 20 and 30 at.% Si.

Figure 4, this phase is described by a sublattice model. Only original, experimentally determined data are indicated. In both variations of the dataset, the agreement between the experimental data of the liquidus and solidus lines and the calculation is generally very high. The calculated liquidus line is largely in good agreement with the experimental data, even though there is little experimental information available on the edges of the system. The solidus lines throughout the system are well represented. The calculated maximum solubility for Si in Mo is calculated to be 4.1 at%, which is in good agreement with the results of a DFT calculation by Lenchuk et al.^[61] Only in case of the solvus line of the Mo–Si solid solution are a few experimental data points which deviate somewhat from the calculation. As part of the optimizations, standard procedures to test the validity

Table 7. Comparison between the experimentally determined values of the temperatures and Si concentrations of the liquid phase for the invariant reactions in the Mo–Si system with the assessed values of this work.

Reaction	Temperature [K]		x(Si)	
	This work	Experimental ^[19]	This work	Experimental ^[19]
$\beta + L \rightleftharpoons \text{Mo}_3\text{Si}$	2301	2298 ± 20	0.248	0.257
$L \rightleftharpoons \text{Mo}_3\text{Si} + \text{Mo}_5\text{Si}_3$	2301	2293 ± 20	0.250	0.264
$L \rightleftharpoons \text{Mo}_5\text{Si}_3$	2452	2453 ± 20	0.375	0.375
$L \rightleftharpoons \text{Mo}_5\text{Si}_3 + \text{MoSi}_2$	2181	2173 ± 20	0.543	0.540
$L \rightleftharpoons \text{MoSi}_2$	2292	2293 ± 20	0.666	0.666
$L \rightleftharpoons \text{Si} + \text{MoSi}_2$	1674	1673 ± 10	0.975	0.985

Table 8. Comparison of the enthalpies of formation of the intermetallic compounds at 298 K in different thermodynamic assessments, calculations, and experimental measurements. All values in kJ mol^{-1} and referred to one mole of atoms.

Literature	Phase			Method
	Mo_3Si	Mo_5Si_3	MoSi_2	
This work	-29.3	-38.2	-43.7	Assessment
Zhong et al. ^[36]	-35.83	-	-	Local density approximation
-	-32.28	-	-	Generalized gradient approximation
Colinet and Tedenac ^[37]	-29.5	-38.44	-47.89	DFT
Guo et al. ^[5]	-29.3	-39.0	-38.3	Assessment
Geng et al. ^[8]	-29.3	-39.0	-43.8	Assessment
Fujiwara and Ueda ^[31]	-30.5 ± 1.5	-39.2 ± 1.5	-45.3 ± 1.5	EMF
Liu et al. ^[7]	-27.9	-39.0	-45.2	Assessment
Meschel and Kleppa ^[62]	-	-38.2 ± 1.6	-47.9 ± 2.1	Direct synthesis calorimetry
Tomaszkiewicz et al. ^[29]	-	-39.3 ± 1.1	-	Combustion calorimetry
Tomaszkiewicz et al. ^[30]	-31.3 ± 1.5	-	-	Combustion calorimetry
Costa e Silva ^[50]	-31.8	-39.2	-45.7	Assessment
Bhaduri et al. ^[34]	-	-38.48	-43.7	Calculation
O'Hare ^[28]	-	-	-45.7 ± 1.5	Combustion calorimetry
Chandrasekharaiah et al. ^[22]	-	-	-45.7 ± 1.3	Assessment
Ohmori et al. ^[63]	-	-37.4 ± 0.1	-	EMF
Niessen and de Boer ^[33]	-26	-	-16.0	Prediction with Miedema model
Machlin ^[66]	-29.6	-	-	Calculation similar to Miedema
Kaufman ^[67]	-39.5	-55.3	-72.1	Prediction
Maslov et al. ^[64]	-	-	-47.4 ± 1.0	Direct synthesis calorimetry
Chart ^[27]	-29.1 ± 3	-38.7 ± 3	-43.9 ± 3	Knudsen effusion
Searcy and Tharp ^[26]	-24.4 ± 4.2	-35.5 ± 7.9	-36.3 ± 13.9	Knudsen effusion
Robins and Jenkins ^[25]	-	(-40.1 ± 1.6)	-43.8 ± 3.3	Combustion calorimetry

Table 9. Comparison of the entropies of formation of the intermetallic compounds at 298 K in different thermodynamic assessments and experimental measurements. All values in $\text{J mol}^{-1} \text{K}^{-1}$ and referred to one mole of atoms.

Literature	Phase			Method
	Mo_3Si	Mo_5Si_3	MoSi_2	
This work	0.284	3.214	0.148	Assessment
Guo et al. ^[5]	-1.3008	-3.5536	-4.29	Assessment
Geng et al. ^[8]	-1.3007	-3.545	-1.84786	Assessment
Fujiwara and Ueda ^[31]	-0.7589	0.55	8.54	EMF
Liu et al. ^[7]	0.28	4.349	-0.223	Assessment
Costa e Silva ^[50]	-2.5	-5.745	-4.2533	Assessment
Vahlas et al. ^[6]	-0.5096	-3.78675	-2.83236	Assessment
Chart ^[27]	0.42 ± 1.3	1.0 ± 1.3	-0.42 ± 1.3	Knudsen effusion
Hultgren et al. ^[68]	0.1 ± 0.3	-0.8 ± 1.3	-2.6 ± 4.2	Assessment

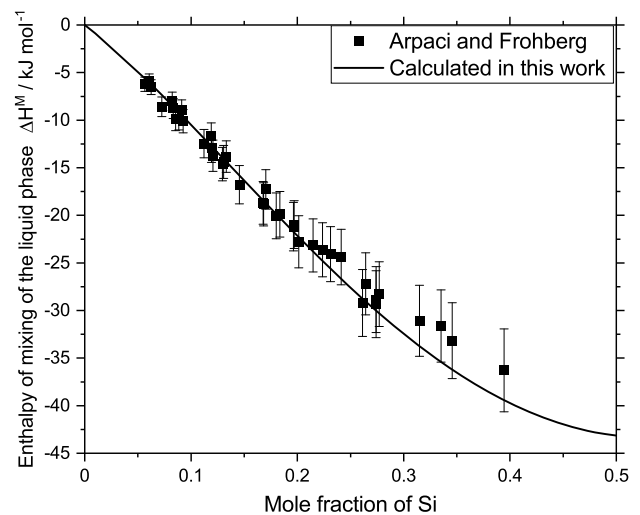


Figure 5. The enthalpy of mixing of the liquid state at a mean temperature of 3087 K. The data points are taken from Arpacı and Froberg,^[42] the line results from the calculation in this work.

of the dataset, such as checking for artificial miscibility gaps in the liquid at very low and high temperatures, were carried out. While an unrealistic miscibility gap in the liquid phase starting at around 4500 K was detected, this issue is negligible due to the unlikelihood that such temperatures are relevant in practice.

Table 7 compares the experimental values and the calculated results of the temperatures and the global Si concentration for each invariant reaction of the system. In all cases, the agreement

between the calculated and the experimental invariant reaction temperatures is very high. All invariant reaction temperatures are very close to the reported value, with a maximum deviation of 3 K. Likewise, the calculated concentrations agree very well with the experimentally determined values in most cases. However, the eutectic reaction $L \rightleftharpoons \text{Si} + \text{MoSi}_2$ shows a somewhat noteworthy deviation of 1 at%. With the given data, no set of parameters could be found that represents all data equally

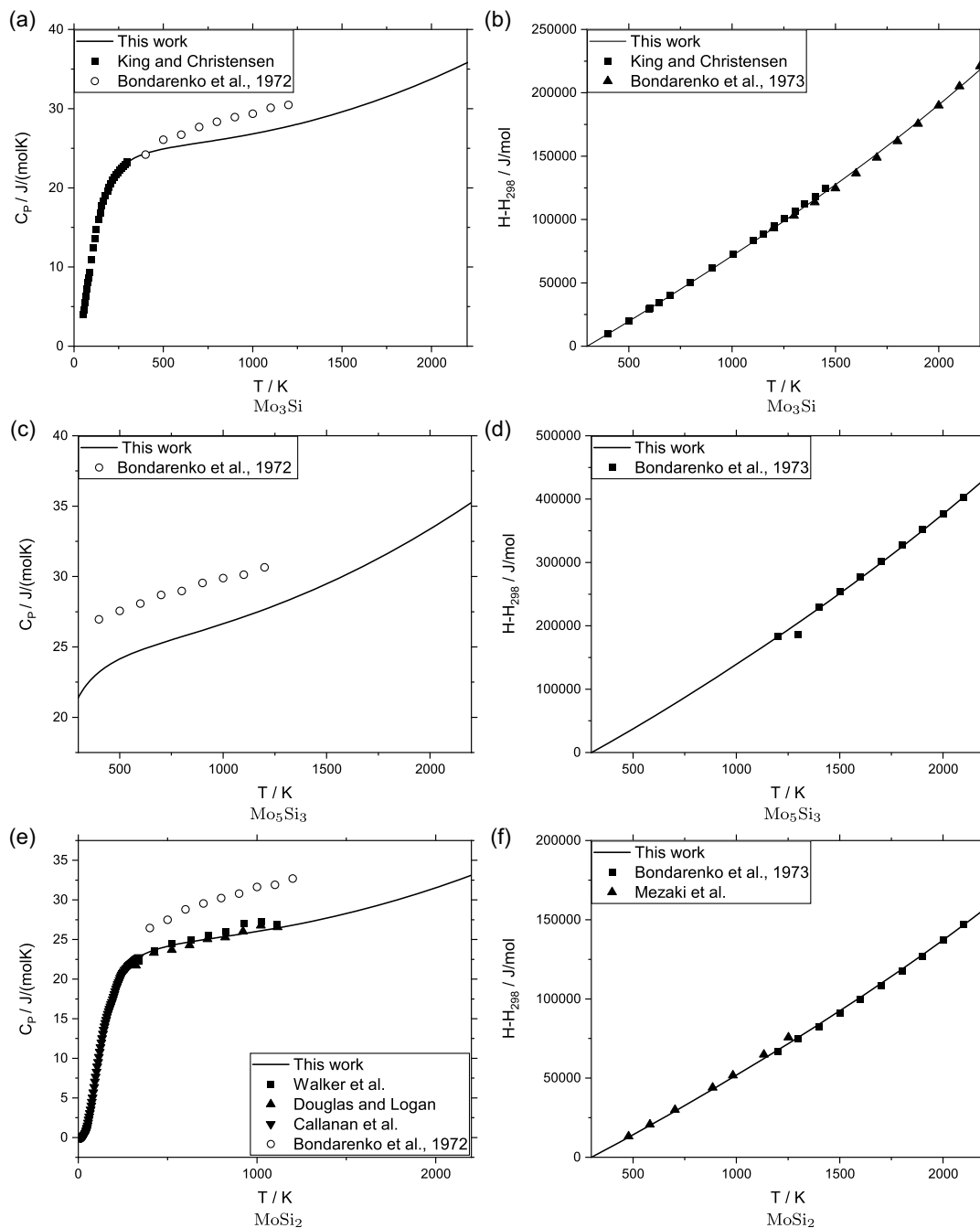


Figure 6. Heat capacities (left column) and enthalpy increments (right column) of the three intermetallic phases. a) and b) correspond to Mo₃Si, c) and d) correspond to Mo₅Si₃ and e) and f) correspond to MoSi₂. The black points are the data used in the optimization^[41,44–48] and the white points correspond to the disregarded experimental data.^[49]

well. Therefore, a compromise had to be found which accounts satisfactory for most of the data. As such, this small discrepancy was accepted, considering the good agreement in all other data.

A comparison between previously reported enthalpies of formation of the silicides at 298 K and the results obtained in this work is given in **Table 8**. As explained in detail in Section 2.2.1, the experiments published by Chart in 1974 are still considered highly reliable, which is why they were chosen for the optimization of the dataset. In addition, the majority of all recent experimental investigations report very similar values. The agreement between the calculation and the experiments is very high for all three intermetallic phases, further emphasizing the reliability of the optimized dataset. The calculated enthalpies of formation at 298 K are $-29.3 \text{ kJ mol}^{-1}$ for Mo_3Si , $-38.2 \text{ kJ mol}^{-1}$ for Mo_5Si_3 and $-43.7 \text{ kJ mol}^{-1}$ for MoSi_2 . The values stated by Chart are $-29.1 \pm 3 \text{ kJ mol}^{-1}$ for Mo_3Si , $-38.7 \pm 3 \text{ kJ mol}^{-1}$ for Mo_5Si_3 , and $-43.9 \pm 3 \text{ kJ mol}^{-1}$ for MoSi_2 . An equally good agreement between calculation and experiment is found for the data at 1500 K: $-28.8 \text{ kJ mol}^{-1}$ for Mo_3Si , $-39.3 \text{ kJ mol}^{-1}$ for Mo_5Si_3 , and $-44.5 \text{ kJ mol}^{-1}$ for MoSi_2 for the calculations versus $-30.1 \pm 3 \text{ kJ mol}^{-1}$ for Mo_3Si , $-38.9 \pm 3 \text{ kJ mol}^{-1}$ for Mo_5Si_3 and $-45.0 \pm 3 \text{ kJ mol}^{-1}$ for MoSi_2 , according to Chart.

Table 9 shows a comparison of the entropies of formation at 298 K between the data given in the literature and in this work. As mentioned in Section 2.2.2, most of these values come from assessments of literature data. The only two sources for experimentally derived values, Chart^[27] and Fujiwara,^[31] reported vastly different results. Chart reported the values $0.42 \pm 1.3 \text{ J mol}^{-1}\text{K}^{-1}$ for Mo_3Si , $1.0 \pm 1.3 \text{ J mol}^{-1}\text{K}^{-1}$ for Mo_5Si_3 , and $-0.42 \pm 1.3 \text{ J mol}^{-1}\text{K}^{-1}$ for MoSi_2 . From the data reported by Fujiwara and Ueda, the values $-0.76 \text{ kJ mol}^{-1} \text{ K}^{-1}$ for Mo_3Si , $0.55 \text{ J mol}^{-1} \text{ K}^{-1}$ for Mo_5Si_3 , and $8.54 \text{ J mol}^{-1}\text{K}^{-1}$ for MoSi_2 can be derived. For this reason, and because of the substantial scatter of the data in previous assessments, no weight was placed on optimizing the dataset with regards to the entropies of formation. Nevertheless, the formation entropies calculated in this work agree quite well with the data reported by Chart for Mo_3Si and MoSi_2 . Only in the case of the phase Mo_5Si_3 is the calculated value slightly lower than Chart's value, including the uncertainty range. Interestingly, the data from **Table 9** indicate that entropies of formation do not seem to have been considered at all in other evaluations of the Mo–Si system in the literature, as the scatter of this parameter is extreme and values do not seem to correspond to experimental results.

Figure 5 shows a comparison between the mixing enthalpy of the liquid phase as reported by Arpacı and Frohberg^[42] and the results calculated with the dataset from this work. The agreement

between calculation and experiment is generally very high, with the entirety of the curve within the experimental uncertainty.

The heat capacities and enthalpy increment data of the intermetallic compounds are shown in **Figure 6**. The lines are the result of this work, while the indicated symbols are data taken from literature.^[41,44–49] Of all the data, only the experiments by Bondarenko et al. in the temperature range from 400 to 1200 K deviate from the calculation. However, as discussed in Section 2.2.4, these data are considered the least reliable of the measurements and were thus not used in the optimization.

In conclusion, the agreement between calculations with the dataset obtained in this work and the experimental measurements is generally very high. The majority of the data, both in terms of phase diagram data and thermophysical parameters, is well-represented by this dataset. Some discrepancies exist in areas where literature data is not considered to be highly reliable. Thus, such data were given low weight for the optimization or even neglected entirely. However, for the most important data, such as the enthalpies of formation and the heat capacities of the silicides, as well the phase diagram data, the calculation is in very good agreement with the experiments.

5. Conclusion

In this work, the thermodynamic description of the Mo–Si system is reevaluated, including data overlooked in previous assessments. Literature data on various properties, such as the enthalpies of formation of the intermetallic phases, invariant reaction temperatures and compositions, and the enthalpy of mixing of the liquid phase, have been discussed and evaluated in terms of the reliability of the measurements. Previous evaluations of the system were taken into account in the modeling of the phases and parameters. All this information was used to write a CALPHAD dataset to calculate the Gibbs energies of all the phases in the system. Two alternative models were used for the Mo_3Si phase. It has been shown that the calculations with the resulting data set are in good agreement with the known data for the Mo–Si system.

In addition, a series of samples were prepared, heat treated, and quenched to confirm the Si deficiency of the phase Mo_3Si reported in the literature. Good agreement was found between the experiments in this work and the literature data.

6. Thermodynamic Parameters

Table 10

Table 10. Optimized thermodynamic parameters of the Mo–Si system. All temperature ranges are from 298.15 to 6000 K.

Phase	Thermodynamic parameters
liquid	Model: (Mo,Si) ${}^0L_{\text{Mo,Si}} = -172591.2920 + 27.6145 T$ ${}^1L_{\text{Mo,Si}} = 26612.6661 - 20.6586 T$ ${}^2L_{\text{Mo,Si}} = 38731.7034$ ${}^3L_{\text{Mo,Si}} = 19624.2756$

Table 10. Continued.

Phase	Thermodynamic parameters
bcc	Model: (Mo,Si) ${}^0L_{\text{Mo,Si}} = -114632.1170 + 26.9372 T$
Mo ₃ Si	Model: (Mo) _{0.77} (Si) _{0.23} $G_{\text{Mo:Si}} = -37759.2536 + 149.3282 T - 26.059 T \ln(T) + 9.6142 \cdot 10^{-4} T^2 - 4.8262 \cdot 10^{-7} T^3 + 113220 T^{-1}$ - OR - Model: (Mo) _{0.75} (Si) _{0.125} (Si, Va) _{0.125} $G_{\text{Mo:Si:Si}} = -37759.2536 + 149.3282 T - 26.059 T \ln(T) + 9.6142 \cdot 10^{-4} T^2 - 4.8262 \cdot 10^{-7} T^3 + 113220 T^{-1}$ $G_{\text{Mo:Si:Va}} = -21414.3469 + 129.4122 T - 22.8016 T \ln(T) + 8.4124 E \cdot 10^{-4} T^2 - 4.2229 \cdot 10^{-7} T^3 + 99067.5 T^{-1}$ ${}^0L_{\text{Mo:Si:Si:Va}} = 0.0$ ${}^1L_{\text{Mo:Si:Si:Va}} = -10750 + 2.5 T$
Mo ₅ Si ₃	Model: (Mo) _{0.5} (Mo, Si) _{0.125} (Mo, Si) _{0.125} (Si) _{0.25} $G_{\text{Mo:Mo:Si:Si}} = -46722 + 143 T - 25.2693 T \ln(T) + 3.2382 \cdot 10^{-4} T^2 - 3.9528 \cdot 10^{-7} T^3 + 1.7454 \cdot 10^5 T^{-1}$ $G_{\text{Mo:Mo:Si:Si}} = -47765 + 147 T - 25.2693 T \ln(T) + 3.2382 \cdot 10^{-4} T^2 - 3.9528 \cdot 10^{-7} T^3 + 1.7454 \cdot 10^5 T^{-1}$ $G_{\text{Mo:Mo:Si:Si}} = -37313 + 146 T - 25.2693 T \ln(T) + 3.2382 \cdot 10^{-4} T^2 - 3.9528 \cdot 10^{-7} T^3 + 1.7454 \cdot 10^5 T^{-1}$ $G_{\text{Mo:Mo:Si:Si}} = -34401 + 140 T - 25.2693 T \ln(T) + 3.2382 \cdot 10^{-4} T^2 - 3.9528 \cdot 10^{-7} T^3 + 1.7454 \cdot 10^5 T^{-1}$
MoSi ₂	Model: (Mo) ₁ (Si) ₂ $G_{\text{Mo:Si}} = -156216.6066 + 444.2883 T - 75.7102 T \ln(T) + 1.6413 \cdot 10^{-3} T^2 - 1.0682 \cdot 10^{-6} T^3 + 402589.974 T^{-1}$

7. Experimental Section

To verify the composition of the Mo₃Si phase experimentally, samples were prepared, heat treated, and quenched in water. Subsequently, the specimens were analyzed by energy dispersive X-ray spectroscopy (EDX), electron probe microanalysis (EPMA) and X-ray diffraction (XRD). This is done to ensure that the assessment of the phase Mo₃Si is supplemented by data based on equilibrated samples with a known history and composition. The materials used in this work were Mo foil (99.95% purity, Alfa Aesar) and Si granulate (99.99% purity, Goodfellow GmbH). Button ingots of 1500 mg were prepared with a non-consumable tungsten electrode using a vacuum arc melter with a water-cooled copper crucible (MAM-1 compact arc furnace Edmund Bühler GmbH). To keep the atmosphere oxygen- and nitrogen-free, the device was situated in a glovebox. Both the arc melter itself and the glovebox were operated using high-purity argon (99.9999 % purity, Alfa Aesar). Prior to arc melting, the materials were weighed carefully to ensure an accurate sample composition. Due to the large difference of the melting points of the elements, the Mo foil was wrapped around the Si granules, so that the molten Mo trapped any Si that may evaporate at high temperatures. Each sample was melted five times to promote complete mixing of the components. Before each melting step, a pure Ti getter was melted and given time to solidify, to reduce the oxygen partial pressure in the melting chamber. After melting, all samples were reweighed to detect potential weight losses during melting.

The heat treatment was conducted in a LORA-GLB tube furnace by HTM Reetz GmbH. The furnace operates with a flowing high-purity argon atmosphere (99.9999%, 0.2 slm flow rate). The gas was additionally purified in an OxiClear - DGP-R1-3000B Purifier by LabClear Inc. before it was led into the furnace. The O₂ concentration of the effluent gas was monitored with an oxygen sensor (E2010 by Zirox GmbH). The heating chamber of the furnace consists of an Al₂O₃ tube. To prevent reactions between the specimens and the tube, the samples were placed in an Al₂O₃ crucible lined with Mo foil. The furnace is built in such a way that the quenching medium is filled into a separate compartment of the device just before quenching. The samples were then dropped into this compartment so that they were not exposed to the environment until they were quenched. The quenching medium used in this work was purified water.

After quenching, the samples were bisected using a diamond blade (DiaCut 007 by Cloeren Technology) in a precision cutting machine (Brillant 220 by ATM Qness GmbH). Subsequently, they were hot-mounted in a conductive medium (WEM REM by Cloeren Technology GmbH, the mounting press was a CitoPress-10 by Struers GmbH). The mounted samples were then polished to a roughness of 0.04 μm. The initial steps of polishing were done using diamond suspensions, the final step used colloidal silica suspension (all polishing media by Cloeren Technology GmbH).

The microstructures of the samples were examined using a Philips XL 30 SFEG scanning electron microscope (SEM) in backscattering mode. The device used to determine the compositions of the phases was a Cameca SX100 electron microprobe. An acceleration voltage of 15 kV was used.

In the event that oxide formation occurred despite the precautions taken during sample preparation and annealing, the entire surface of the sample was mechanically ground prior to XRD analysis. Subsequently, the samples were ground to fine powder using an agate mortar. No attempt was made to determine the particle size of the powder. To investigate the phases present in the samples, an Empyrean X-ray Diffractometer (Malvern Panalytical GmbH) with a PIXCEL3D Medipix3 1x1 detector was used. The measurement was carried out in Bragg-Brentano geometry. As radiation source, a copper cathode with monochromatized CuKα1 radiation was used. The step size of the diffractometer was 0.013°.

Acknowledgements

The authors gratefully acknowledge the funding by the German Research Foundation (DFG) as part of the Research Training Group 2561: Materials Compounds from Composite Materials for Applications in Extreme Conditions.

Open Access funding enabled and organized by Projekt DEAL.

Conflict of Interest

The authors declare no conflict of interest.

Data Availability Statement

The data that support the findings of this study are available from the corresponding author upon reasonable request

Keywords

calculation of phase diagrams, Mo–Si system, phase diagrams, thermodynamic assessments

Received: December 6, 2023

Revised: January 10, 2024

Published online:

- [1] J. Petrovic, A. Vasudevan, *Mater. Sci. Eng. A* **1999**, 261, 1.
- [2] T. C. Chou, T. G. Nieh, *JOM* **1993**, 45, 15.
- [3] U. Waghmare, V. Bulatov, E. Kaxiras, M. Duesbery, *Mater. Sci. Eng. A* **1999**, 261, 147.
- [4] G.-J. Zhang, X.-H. Lin, R.-H. Wang, G. Liu, J. Sun, *Int. J. Refract. Met. Hard Mater.* **2011**, 29, 608.
- [5] C. Guo, C. Li, P. J. Masset, Z. Du, *Calphad* **2012**, 36, 100.
- [6] C. Vahlas, P. Y. Chevalier, E. Blanquet, *Calphad* **1989**, 13, 273.
- [7] Y. Liu, G. Shao, P. Tsakiroopoulos, *Intermetallics* **2000**, 8, 953.
- [8] T. Geng, C. Li, X. Zhao, H. Xu, Z. Du, C. Guo, *Calphad* **2010**, 34, 363.
- [9] I. Rosales, J. H. Schneibel, *Intermetallics* **2000**, 8, 885.
- [10] A. Gulec, X. Yu, M. Taylor, J. H. Perepezko, L. Marks, *Acta Crystallogr. A* **2016**, 72, 660.
- [11] I. Gnesin, B. Gnesin, *Int. J. Refract. Met. Hard Mater.* **2020**, 88, 105188.
- [12] D. Schliephake, A. Kauffmann, X. Cong, C. Gombola, M. Azim, B. Gorr, H.-J. Christ, M. Heilmaier, *Intermetallics* **2019**, 104, 133.
- [13] S. Katrych, A. Grytsiv, A. Bondar, P. Rogl, T. Velikanova, M. Bohn, *J. Alloys Compd.* **2002**, 347, 94.
- [14] H. Wu, C. Li, C. Guo, Z. Du, *J. Alloys Compd.* **2022**, 922, 166164.
- [15] A. B. Gokhale, G. J. Abbaschian, *J. Phase Equilib.* **1991**, 12, 493.
- [16] M. E. Schlesinger, *Chem. Rev.* **1990**, 90, 607.
- [17] J. L. Ham, *Trans. Am. Soc. Mech. Eng.* **1951**, 73, 723.
- [18] R. Kieffer, E. Cerwenka, *Z. Metallke.* **1952**, 43, 101.
- [19] V. N. Svechnikov, Y. A. Kocherzhinskii, L. M. Yupko, *Diagrammy Sostojanija Metallicheskich Sistem*, Nauka, Moscow **1971**.
- [20] P. Frankwicz, J. Perepezko, *Mater. Sci. Eng. A* **1998**, 246, 199.
- [21] G. B. Cherniak, A. G. Elliot, *J. Am. Ceramic Soc.* **1964**, 47, 136.
- [22] M. S. Chandrasekharaiyah, J. L. Margrave, P. A. G. O'Hare, *J. Phys. Chem. Ref. Data* **1993**, 22, 1459.
- [23] *Atomic Energy Review, Special Issue No. 7 Molybdenum: Physico-Chemical Properties of its Compounds and Alloys* (Ed: L. Brewer), International Atomic Energy Agency, Vienna **1980**.
- [24] T. G. Chart, *High Temp. - High Press.* **1973**, 5, 241.
- [25] D. A. Robins, I. Jenkins, *Acta Metall.* **1955**, 3, 598.
- [26] A. W. Searcy, A. G. Tharp, *J. Phys. Chem.* **1960**, 64, 1539.
- [27] T. G. Chart, *Met. Sci.* **1974**, 8, 344.
- [28] P. A. G. O'Hare, *J. Chem. Thermodyn.* **1993**, 25, 1333.
- [29] I. Tomaszewicz, G. A. Hope, C. M. Beck II, P. A. G. O'Hare, *J. Chem. Thermodyn.* **1997**, 29, 87.
- [30] I. Tomaszewicz, G. A. Hope, C. M. Beck II, P. A. G. O'Hare, *J. Chem. Thermodyn.* **1996**, 28, 29.
- [31] H. Fujiwara, Y. Ueda, *J. Alloys Compd.* **2007**, 441, 168.
- [32] A. Miedema, P. de Châtel, F. de Boer, *Physica B+C* **1980**, 100, 1.
- [33] A. K. Niessen, F. R. de Boer, *J. Less-Common Met.* **1981**, 82, 75.
- [34] S. B. Bhaduri, Z. B. Qian, R. Radhakrishnan, *Scr. Metall. Mater.* **1994**, 30, 179.
- [35] I. Barin, *Thermochemical Data of Pure Substances*, VCH Verlagsgesellschaft mbH, Weinheim, Germany, **1989**.
- [36] S. Zhong, Z. Chen, M. Wand, D. Chen, *Eur. Phys. J. B* **2016**, 89, 6.
- [37] C. Colinet, J.-C. Tedenac, *Calphad* **2016**, 54, 16.
- [38] Y. Pan, *J. Alloys Compd.* **2019**, 779, 813.
- [39] A. T. Dinsdale, *Calphad* **1991**, 15, 317.
- [40] J. E. Callanan, R. D. Weir, E. F. Westrum Jr., *J. Chem. Thermodyn.* **1996**, 28, 1233.
- [41] E. G. King, A. U. Christensen Jr., *J. Phys. Chem.* **1958**, 62, 499.
- [42] E. Arpacı, M. G. Froberg, *Z. Metallke.* **1985**, 76, 440.
- [43] V. S. Sudavtsova, G. I. Batalin, V. S. Tutevich, *Russ. J. Phys. Chem.* **1985**, 59, 1282.
- [44] T. B. Douglas, W. M. Logan, *J. Res. Natl Bur. Stand.* **1954**, 53, 91.
- [45] J. E. Callanan, R. D. Weir, E. F. Westrum Jr., *Pure Appl. Chem.* **1997**, 69, 2289.
- [46] B. E. Walker, J. A. Grand, R. R. Miller, *J. Phys. Chem.* **1956**, 60, 231.
- [47] R. Mezaki, E. W. Tilleux, T. F. Jambois, J. L. Margrave, *High-Temperature Thermodynamic Functions for Refractory Compounds*, American Society of Mechanical Engineers, New York, **1965**.
- [48] V. P. Bondarenko, E. N. Fomichev, A. A. Kalashnik, *Heat Transfer-Sov. Res.* **1973**, 5, 76.
- [49] V. P. Bondarenko, P. N. V'yugov, V. I. Zmii, A. S. Knyazhev, *Teplofiz. Vys. Temp.* **1972**, 10, 1013.
- [50] A. Costa e Silva, Ph.D. thesis, University of Florida, Gainesville, FL **1994**.
- [51] P. B. Fernandes, G. C. Coelho, F. Ferreira, C. A. Nunes, B. Sundman, *Intermetallics* **2002**, 10, 993.
- [52] M. Hillert, L. Staffansson, *Acta Chem. Scand.* **1970**, 24, 3618.
- [53] M. Hillert, *J. Alloys Compd.* **2001**, 320, 161.
- [54] H. L. Lukas, S. G. Fries, B. Sundman, *Computational Thermodynamics - The Calphad Method*, Cambridge University Press, New York, USA **2007**.
- [55] P. Villars, L. D. Calvert, *Pearson's Handbook of Crystallographic Data for Intermediate Phases*, American Society of Metals, Cleveland, OH **1985**.
- [56] H. L. Zhao, M. J. Kramer, M. Akinc, *Intermetallics* **2004**, 12, 493.
- [57] D. H. Templeton, C. H. Dauben, *Acta Crystallogr.* **1950**, 261.
- [58] M. Aindow, L. S. Smith, J. Shyue, M. H. Loretto, H. L. Fraser, *Philos. Mag. Lett.* **1994**, 69, 23.
- [59] S. Prasad, A. Paul, *Intermetallics* **2011**, 19, 1191.
- [60] B. Sundman, B. Jansson, J.-O. Andersson, *Calphad* **1985**, 9, 153.
- [61] O. Lenchuk, J. Rohrer, K. Albe, *Scr. Mater.* **2015**, 97, 1.
- [62] S. V. Meschel, O. J. Kleppa, *J. Alloys Compd.* **1998**, 274, 193.
- [63] S. Ohmori, Y. Hashimoto, K. Kohyama, *J. High Temp. Soc. Jpn.* **1982**, 8, 113.
- [64] V. M. Maslov, A. S. Neganov, I. P. Borovinskaya, A. G. Merzhanov, *Combust. Explos. Shock Waves* **1978**, 14, 759.
- [65] D. Birnie, E. S. Machlin, L. Kaufman, K. Taylor, *Calphad* **1982**, 6, 93.
- [66] E. S. Machlin, *Calphad* **1981**, 5, 1.
- [67] L. Kaufman, *Calphad* **1979**, 3, 45.
- [68] R. Hultgren, P. D. Desai, D. T. Hawkins, M. Gleiser, K. K. Kelley, Selected values of the thermodynamic properties of the elements, Technical report, National Standard Reference Data System, **1973**.